Development and Application of External Electric Fields for Advanced Polarizable Force Fields

Moses K. J. Chung,[1, a)] Rebecca A. Bone,[2, 3, a)] Zhi Wang,[1, a)] Kathleen Schwarz,[3, b)] and Jay W. Ponder[1, c)]
[1)] *Department of Chemistry, Washington University in St. Louis, St. Louis, MO 63130, United States*
[2)] *Theiss Research, P.O. Box 127, La Jolla, California, 92038, United States*
[3)] *Material Measurement Laboratory, National Institute of Standards and Technology, 100 Bureau Dr., Gaithersburg, Maryland 20899, United States*

(Dated: 11 August 2026)

External electric fields can dramatically alter the structure and dynamics of molecules and materials. The electric field response involves both the direct electrostatics and the polarization of the molecule. The polarization term is not included in non-polarizable force fields, yet it is key to correctly describing the response. Here, we implement static and oscillating external electric fields in the Tinker molecular dynamics software for use with polarizable force fields. We demonstrate the implementation through dielectric spectra of water, dielectric spectra of an aqueous glucose solution, and trajectory analysis of an amyloid beta protein.

INTRODUCTION

In molecular dynamics (MD) simulations, external electric fields can be applied to examine how molecular systems respond to controlled field perturbations. External field simulations have been used to investigate a wide range of phenomena, such as diffusion enhancement[1], dielectric spectra calculations[2], and biomolecular structural changes[3]. External field simulations offer a method to perturb systems and allow accurate modeling of systems found in nature. There exists a rich history of external field MD simulations that we cannot fully delineate here; however, we highlight a few interesting examples below.

External fields are instrumental in Stark spectroscopy, which allows measurement of electric fields in molecules and is used to study enzyme catalysis[4–6]. When simulating the diffusion of water through the aquaporin-4 channel, the filter is kinetically inaccessible in the absence of a field[7]. It has been shown that field conditions can affect proteins in paradoxical ways, sometimes stabilizing certain conformational states and other times denaturing them[3]. External field simulations have also been helpful in probing physicochemical systems[8]. Specifically, we have previously demonstrated a method for computational dielectric spectroscopy based on the direct application of an oscillating electric field.[9] This method allows a straightforward connection between the configurational changes seen in solution and the dielectric response of the medium, a useful feature when identifying mechanisms of dielectric response.[10] Additionally, when an applied electric field is of large enough magnitude, the nonlinear dielectric effects on the simulation may also be probed[9,11].

These applications ultimately depend on how the external field energies are modeled. External electric fields interact with molecules through two energy terms, direct Coulomb electrostatics and shifts in the charge distribution, resulting in polarization energy. To improve the treatment of polarization in external field MD simulations and accessibility of these methods to the modeling community, we implemented static and oscillating external electric fields for the polarizable force fields AMOEBA[12], AMOEBA+[13], and HIPPO[14] in the Tinker-CPU[15] and Tinker-GPU[16] packages. We demonstrate two applications of external field MD simulations: dielectric spectra calculations and field induced disorder of an amyloid protein. Our simulations capture features of the dielectric spectrum of water and that of aqueous glucose solutions, in qualitative agreement with experimental findings. For the external field amyloid simulations, our results reproduce the frequency dependent denaturation of the amyloid beta protein[17].

METHODS

Electrostatic and Polarization Energy Implementation

We incorporated the external electric field routines in Tinker-CPU[15] and Tinker-GPU[16]. Here, we briefly derive the electrostatic and polarization energy arising from external fields. The electrostatic energy due to an external field is

$$U_{ele} = \int \rho(\mathbf{r})\, V(\mathbf{r})\, d^3r, \tag{1}$$

where ρ is the charge distribution and V is the potential due to the electric field. We expand the potential about the origin of an atom at $\mathbf{r}_0$

$$V(\mathbf{r}_0 + \mathbf{r}) = V(\mathbf{r}_0) + r_i\, \partial_i V(\mathbf{r}_0) + \frac{1}{2} r_i r_j\, \partial_i \partial_j V(\mathbf{r}_0) + \cdots, \tag{2}$$

[a)] These authors contributed equally to this work.
[b)] Electronic mail: kathleen.schwarz@nist.gov; Corresponding authors.
[c)] Electronic mail: ponder@dasher.wustl.edu; Corresponding authors.

and substitute it into the electrostatic energy to obtain

$$U_{ele} = V(\mathbf{r}_0)\int \rho\, d^3r + \partial_i V(\mathbf{r}_0)\int \rho\, r_i\, d^3r + \frac{1}{2}\partial_i\partial_j V(\mathbf{r}_0)\int \rho\, r_i r_j\, d^3r + \cdots . \quad (3)$$

With the reference $V(\mathbf{0}) = 0$, we obtain $V(\mathbf{r}_0) = -\mathbf{r}_0 \cdot \mathbf{E}^{ext}$ and $\partial_i V(\mathbf{r}_0) = -E_i^{ext}$, where $\mathbf{E}^{ext}$ is the external electric field. For a uniform electric field, the $\partial_i\partial_j V(\mathbf{r}_0)$ and higher order terms drop out. Replacing the charge distribution integrals with monopole q and dipole $\mathbf{p}$, we obtain the electrostatic energy:

$$U_{ele} = -q(\mathbf{r}_0 \cdot \mathbf{E}^{ext}) - \mathbf{p} \cdot \mathbf{E}^{ext}. \quad (4)$$

For the AMOEBA family of force fields, the external electric field contributes to the polarization energy via the induced dipoles. The induced dipoles are solved iteratively from

$$\boldsymbol{\mu} = \alpha(\mathbf{E}^{perm} + \mathbf{E}^{ind}), \quad (5)$$

where $\boldsymbol{\mu}$ is the induced dipole, α is atomic polarizability, $\mathbf{E}^{perm}$ is the permanent electric field, and $\mathbf{E}^{ind}$ is the electric field from induced dipoles. Both the atomic multipoles and external electric field contribute to the permanent electric field:

$$\mathbf{E}^{perm} = \mathbf{E}^{mpole} + \mathbf{E}^{ext}. \quad (6)$$

In practice, the permanent electric field $\mathbf{E}^{perm}$ is first computed and the induced dipole is iteratively solved by Eq. 5 as described in previous work[15,18].

Dielectric Spectrum Simulation Setup

We compare three force fields for water: AMOEBA[12], AMOEBA+[13], and HIPPO[14] as parameterized in the water03.prm, amoebaplus.prm, and water22.prm files in the Tinker-CPU distribution. For each force field, we generate an initial configuration consisting of 500 molecules using Packmol[19].

For water/glucose simulations, we use the parameterization of the two anomers of glucose in Ref. 20. For the 2 mol/L glucose solution, we used Packmol to construct a simulation box consisting of 9 alpha glucose, 16 beta glucose, and 535 water molecules. The anomers cannot interconvert in simulations.

All simulations are equilibrated for 5 ns in the isothermal-isobaric (NPT) ensemble using the Nosé-Hoover thermostat and barostat[21]. Van der Waals interactions are smoothed to zero at a 9 Å cutoff, and particle mesh Ewald interactions are cut off at 7 Å. Self-consistent mutual polarization is included. A time step of 1 fs is used for all simulations.

Thermostat testing

To test the performance of the Bussi[22] and Nosé-Hoover[21] thermostats with an applied field, we constructed five simulation boxes containing 500 water molecules and five simulation boxes containing 5000 water molecules, 90 sodium ions, and 90 chloride ions, all with Packmol. Each box is equilibrated with no applied field at 300 K and 1 atm separately using the Bussi and the Nosé-Hoover thermostats, otherwise using the equilibration procedure above. Then, each of the five replicates is simulated with no field, a field of 0.001 V/Å strength, a field of 0.01 V/Å strength, and a field of 0.1 V/Å for 5 ns. At each field strength the simulation boxes are simulated at frequencies of 0.1 GHz, 1 GHz, 10 GHz, 100 GHz, and 1000 GHz. Following this 5 ns simulation, each box is simulated for 1 time step in Tinker-CPU to obtain the final temperature. The arithmetic mean of the final temperature of 5 independent simulations is reported together with one standard deviation.

Fluctuation Dissipation Theorem

To calculate a dielectric spectrum using the Fluctuation Dissipation Theorem method, a single equilibrated box is simulated for 50 ns for all water simulations and 500 ns for the water/glucose system in the NPT ensemble using the Nosé-Hoover thermostat and barostat. At each 1 fs time step of the simulation, the polarization of the simulation box is collected in each dimension. This polarization is then used to calculated the dielectric spectrum as in Ref. 23.

Direct Electric Field

To calculate the dielectric spectrum by direct application of an electric field, replicates of the equilibrated simulation box are each subsequently equilibrated in the presence of an oscillating electric field of strength 0.01 V/Å for 5 ns. For in-field simulations, we use the Bussi thermostat and the Monte Carlo barostat[24], because the Monte Carlo barostat allows a virial independent pressure equilibration. Each in-field equilibrated box is then simulated for 100 cycles of the electric field, and we record the polarization at 50 points, evenly spaced in time, per cycle. The polarization of water and glucose are also collected separately for the dissection of the spectrum, as in Ref. 25. The permittivity is then calculated as in Ref. 9. For water spectra, simulations were performed for frequencies of 0.1 GHz, 0.2 GHz, 0.5 GHz, 1 GHz, 2 GHz, 5 GHz, 10 GHz, 20 GHz, 50 GHz, 100 GHz, 200 GHz, 500 GHz, and 1000 GHz. For the water/glucose spectrum, simulations were performed at frequencies of 0.05 GHz, 0.08 GHz, 0.09 GHz, 0.1 GHz, 0.2 GHz, 0.3 GHz, 0.4 GHz, 0.5 GHz, 0.8 GHz, 0.9 GHz, 1 GHz, 2 GHz, 3 GHz, 4 GHz, 5 GHz, 8 GHz, 9 GHz, 10 GHz, 20 GHz, 30 GHz,

40 GHz, 50 GHz, 80 GHz, 90 GHz, 100 GHz, 200 GHz, 300 GHz, 400 GHz, 500 GHz, 800 GHz, 900 GHz, and 1000 GHz.

Debye Peak Fitting

We fit the imaginary component of the experimental water spectrum, the experimental water/glucose spectra, and the simulated water/glucose spectra to a single Debye peak according to the equation:

$$\chi''(f) = \frac{\Delta\epsilon_D f/f_D}{1+(f/f_D)^2}, \tag{7}$$

where χ'' is the imaginary component of the susceptibility (related to the permittivity $\epsilon = \chi+1$), f is frequency, $\Delta\epsilon_D$ is the magnitude of the Debye peak's contribution to the real component of the permittivity, and f_D is the frequency of the Debye peak. We do not analyze the other peaks in the spectra.

Amyloid Beta Simulation Setup

From the cryo-EM structure of the amyloid beta 1–42 fibril[26] (PDB: 5OQV), a pentamer segment from one side of the filament was converted to AMOEBA xyz format to be used with the AMOEBABIO18 force field[27]. The pentamer was rotated to its inertial frame, solvated in a 70 Å x 70 Å x 70 Å cubic water box, 15 sodium ions were added to neutralize the box, and the structure was minimized to 2 kcal/mol/Å (where 1 kcal/mol ≈ 0.043 eV). Using Tinker-GPU, the simulations were set up with the following settings. The equations of motion were integrated for 140 ns using a two stage RESPA integrator[28] with inner 0.25 fs and outer 2 fs time steps. The amyloid protein was simulated with no electric field, a static 0.02 V/Å field, and an oscillating 0.02 V/Å field at 0.01 GHz, 0.1 GHz, and 1 GHz. The isothermal isobaric ensemble (NPT) at 298 K and 1 atm was maintained using a Bussi thermostat and a Monte Carlo barostat. Trajectories were analyzed with MDTraj[29] and visualized with PyMOL[30]. At the end of each simulation, the temperature was averaged over 100 MD steps using Tinker-CPU with the keyword "tau-temperature 10000", setting the half-life for temperature equilibration to 10000 steps and effectively disabling thermostating during those steps.

RESULTS AND DISCUSSION

Polarization Energy

Both the electrostatic and polarization energies are needed to describe the energetics of the system. To illustrate this point, we consider a simple system of water molecules in an external field of 0.02 V/Å. In this system of a minimized 50 Å x 50 Å x 50 Å cubic box of 4167 water molecules, the electrostatic energy decreases 4.6 kcal/mol and the polarization energy decreases by 5.3 kcal/mol for the AMOEBA03 force field[12]. Thus, the magnitudes of both energy components are roughly equivalent, motivating the need for polarizable force fields.

TABLE I. Average final temperature of 5 simulations of water using the Bussi thermostat set to 298 K during application of 0.1 V/Å electric field

Frequency (GHz)	Time constant (ps)	Final temperature (K)
0.1	0.2	298.9 ± 7.5
1.0	0.2	301.8 ± 6.4
10.0	0.2	297.0 ± 5.5
100.0	0.2	297.3 ± 2.4
1000.0	0.2	312.1 ± 4.3
1000.0	0.02	297.3 ± 3.5

Thermostat for External Field Simulation

The application of an electric field to a medium can result in dielectric heating if the field is sufficiently strong. At the same time that we apply electric fields to simulations, we are using a thermostat. This thermostat is meant to keep the simulation at a constant temperature. We test the performance of two common thermostats (Bussi[22] and Nosé-Hoover[21]) for a pure water system and a system with a strong electrolyte (1 mol/kg NaCl) by comparing the temperature in several simulations with and without an applied electric field at various frequencies, as described above.

We find that for relatively low field strengths (0.001 V/Å and 0.01 V/Å), both the Bussi and Nosé-Hoover thermostats are able to maintain a consistent temperature across a wide variety of frequencies (0.1 GHz to 1 THz) when the default time constants in Tinker-GPU[16] are used (0.2 ps for Bussi and 1 ps for Nosé-Hoover) for both pure water systems and strong electrolyte systems (see Supplementary Material). However, we observe inconsistent heating of the simulations at elevated field strength (0.1 V/Å) and frequency (100 GHz and 1 THz) for both thermostats in both pure water (Table I) and electrolyte systems (see Supplementary Material). Adjusting the time constants down by one order of magnitude (0.02 ps for Bussi and 0.1 ps for Nosé-Hoover) is sufficient to maintain the set temperature without heating in a pure water system. However, the Nosé-Hoover thermostat requires additional reduction of the time constant down to 0.02 ps in order to maintain the set temperature when a high strength and high frequency field is applied to a strong electrolyte solution.

Water Spectra

We have determined the dielectric spectrum of water using the AMOEBA[12], AMOEBA+[13], and HIPPO[14] force fields from both a single equilibrium simulation using the FDT method and from simulations in which an electric field is applied at a particular frequency. As shown in Figure 1, the calculated spectra for all force fields, both from FDT and from the application of a field, have all six of the peaks observed in experimental spectra (obtained from Refs. 31–40. Further, the magnitude and location of the Debye peak, the lowest frequency and highest magnitude peak in water's spectrum, is well-captured with each of these force fields for both methods, as reported previously for the AMOEBA force field[23].

Water/Glucose Spectra

Next, we demonstrate spectral decomposition of a model system, a 2 mol/L aqueous solution of glucose. This system is relevant for biological applications, primarily blood-glucose level monitoring for the treatment of diabetes. The decrease in magnitude and frequency of the Debye peak calculated from equilibrium and from in-field simulations (Fig. 2a) are in good agreement with one another. They are also in very good agreement with the experimental glucose spectra reported in Ref. 41 and a fit of the composite experimental water spectrum from Fig. 1, as shown in Fig. 2c-d. Additionally, our simulated spectra have another feature in the spectrum at frequencies below the Debye peak. It is unclear whether this feature is due to a limitation in the force field or our simulation, or if there is actually a feature in the experimental spectrum, given the disagreement in experimental spectra among those of Refs. 37,41–43, that in Ref. 44, and the fits of spectra reported in Ref. 45.

We can also decompose our spectra into the individual contributions from water and glucose, as shown in Figure 2b. We see that both the glucose and the water contribute to both the Debye peak and to the possible low frequency peak. Focusing on the Debye peak, in water this peak is generally attributed to "collective motion" of the hydrogen-bonding network[46,47]. In solutions such as water/alcohol mixtures, hybrid hydrogen-bonding networks form[48]. Species in these hybrid networks respond at a shared frequency, as seen in the decomposed dielectric spectra of water/alcohol mixtures[25]. The decomposed water-glucose spectrum suggests that glucose and water may similarly form a hybrid hydrogen-bonding network, with both water and glucose contributing to this spectral feature.

Electric Field Induced Disordering of Amyloid Beta

External electric fields have been established as therapies for conditions including glioblastoma (tumor treating fields)[49] and Parkinson's disease (deep brain stimulation)[50]. Emerging experimental[51] and computational[17] studies suggest that external electric fields may also be used to treat Alzheimer's disease by solubilizing amyloid beta 1-42, although this possibility remains at an early, preclinical stage. As an example of external electric field protein simulation, we simulated the amyloid beta protein with no electric field, static electric field, and os-

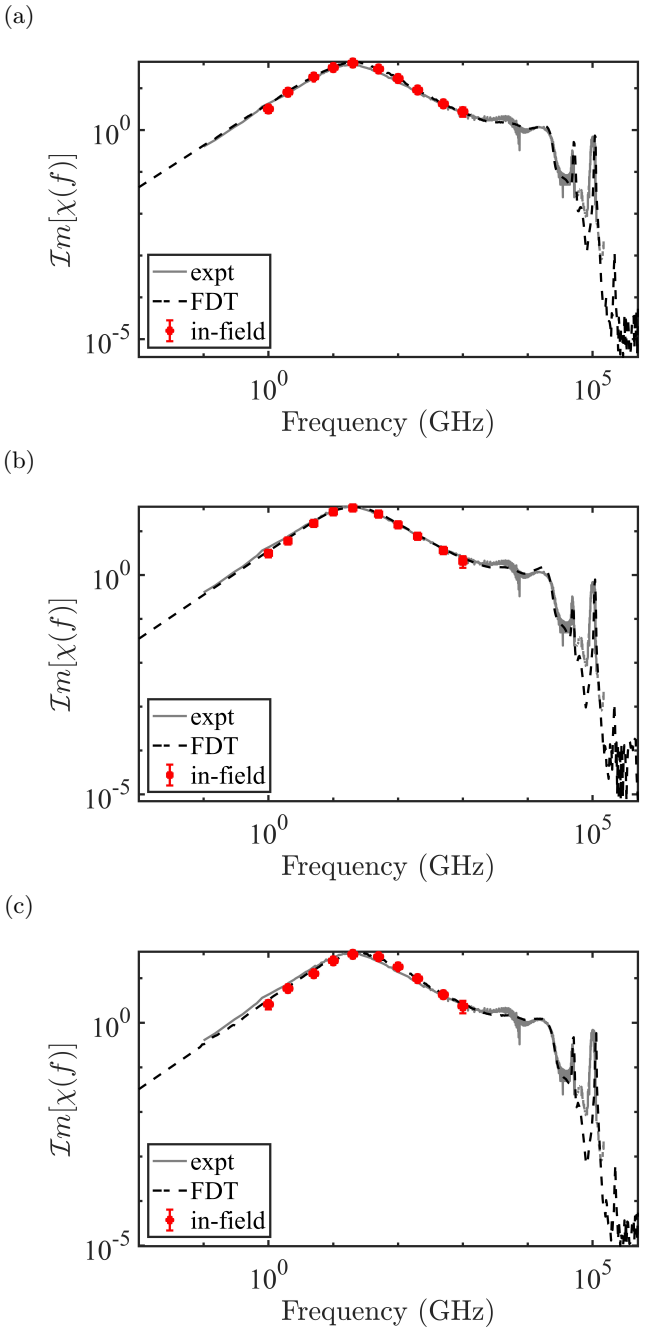

FIG. 1. Imaginary component of the dielectric spectrum of water from experiments in Refs. 31–40 (gray), FDT (black), and direct field application (red) using the (a) AMOEBA, (b) AMOEBA+, and (c) HIPPO force fields.

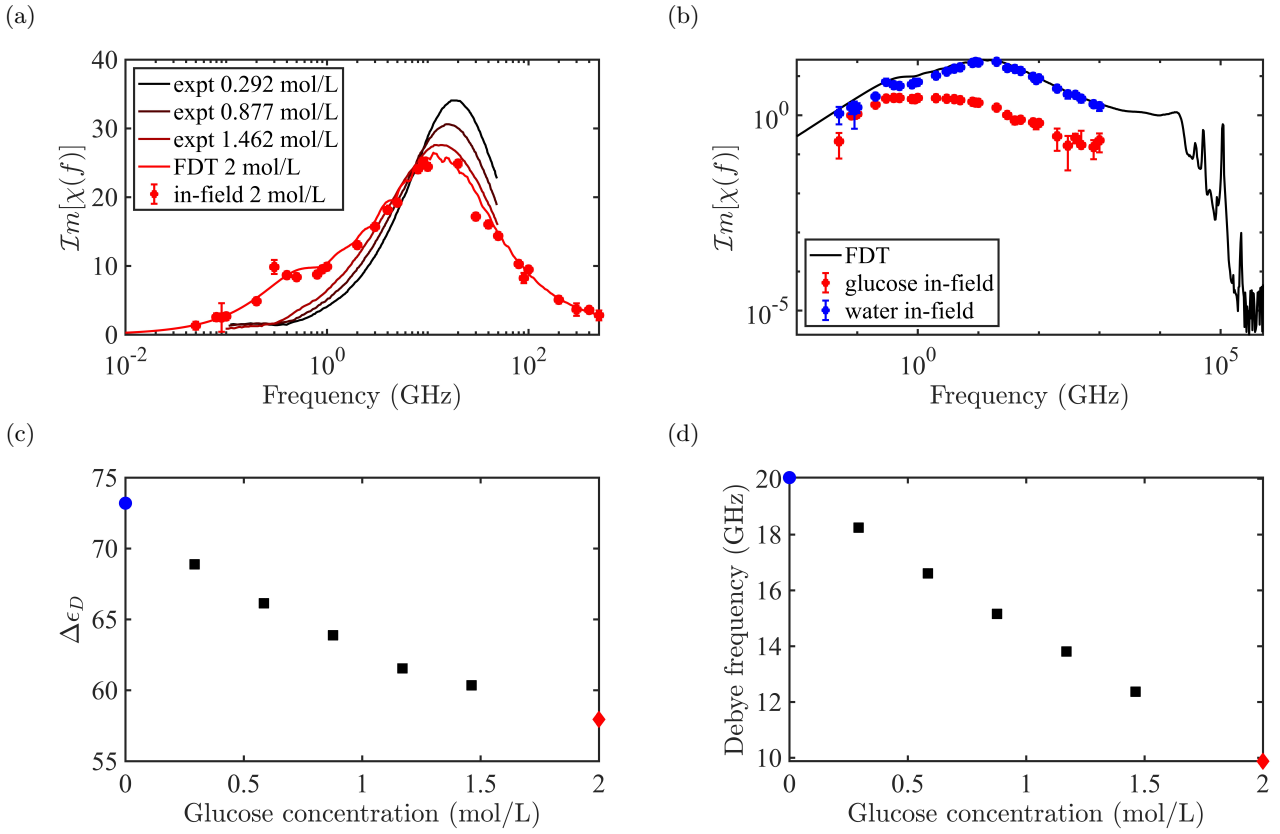

FIG. 2. (a) Imaginary component of the dielectric spectrum of aqueous glucose from experiments in Ref. 41, FDT calculation, and in-field simulations. (b) Component analysis of in-field spectrum. (c) Magnitude of the Debye peak's contribution to the real component of the permittivity $\Delta\epsilon_D$ and (d) frequency of the Debye peak from our fit of the Debye peak in water and water/glucose spectra. Experimental water from Refs. 31–40 (blue circle), experimental water/glucose mixtures from Ref. 41 (black squares), and simulated water/glucose mixture (red diamond).

cillating electric field and analyzed the resulting 140 ns trajectories for disorder as indicated by beta sheet fraction, solvent-accessible surface area (SASA), hydrogen bond count, and root mean square deviation (RMSD).

Snapshots of the amyloid protein simulations with the electric field applied in the x-direction are shown in Figure 3. By 140 ns, all simulations, including no electric field, static field, and oscillating field cases, show structural disorder. However, the rate and extent of this disorder differ markedly between the simulations. The no field simulation remains relatively stable until 60 ns, whereas the 0.02 V/Å 0.1 GHz simulation is already highly disordered at the same time point. Although this relative stability can be seen from the snapshots, direct comparison across the static and oscillating field simulations is difficult. We therefore computed the beta sheet fraction, SASA, hydrogen bond count, and RMSD (Figure 4), which together provide a clearer comparison between the simulations.

Based on these structural metrics, the no electric field simulation was the most stable, while the 0.02 V/Å 0.1 GHz simulation showed greatest disorder. The metrics for the static, 0.01 GHz, and 1 GHz simulations fell between these two cases. A similar trend was reported in Ref. 17, where a frequency dependent response was observed, with a moderate frequency producing faster and greater disorder than either low or high frequencies. Compared to that study, our no field simulation is less stable. It remains to be determined which energy terms drive these differences between the two force fields, whether from valence or non-valence contributions. The inclusion of multipoles and polarization is an obvious distinction between the force fields, but a more detailed analysis is needed to identify the primary source of the difference.

We also report fields applied along the y- and z-axes, shown in Supplementary Figures 1, 2, 3, and 4. These followed trends similar to the X axis simulations. However, because each simulation in this study was run once, future work with replicates may be needed to validate the observations. Finally, to assess potential dielectric heating, we computed the temperature at the end of each simulation, which averaged 298.35 K (Supplementary Table XXI), close to the thermostat target of 298 K.

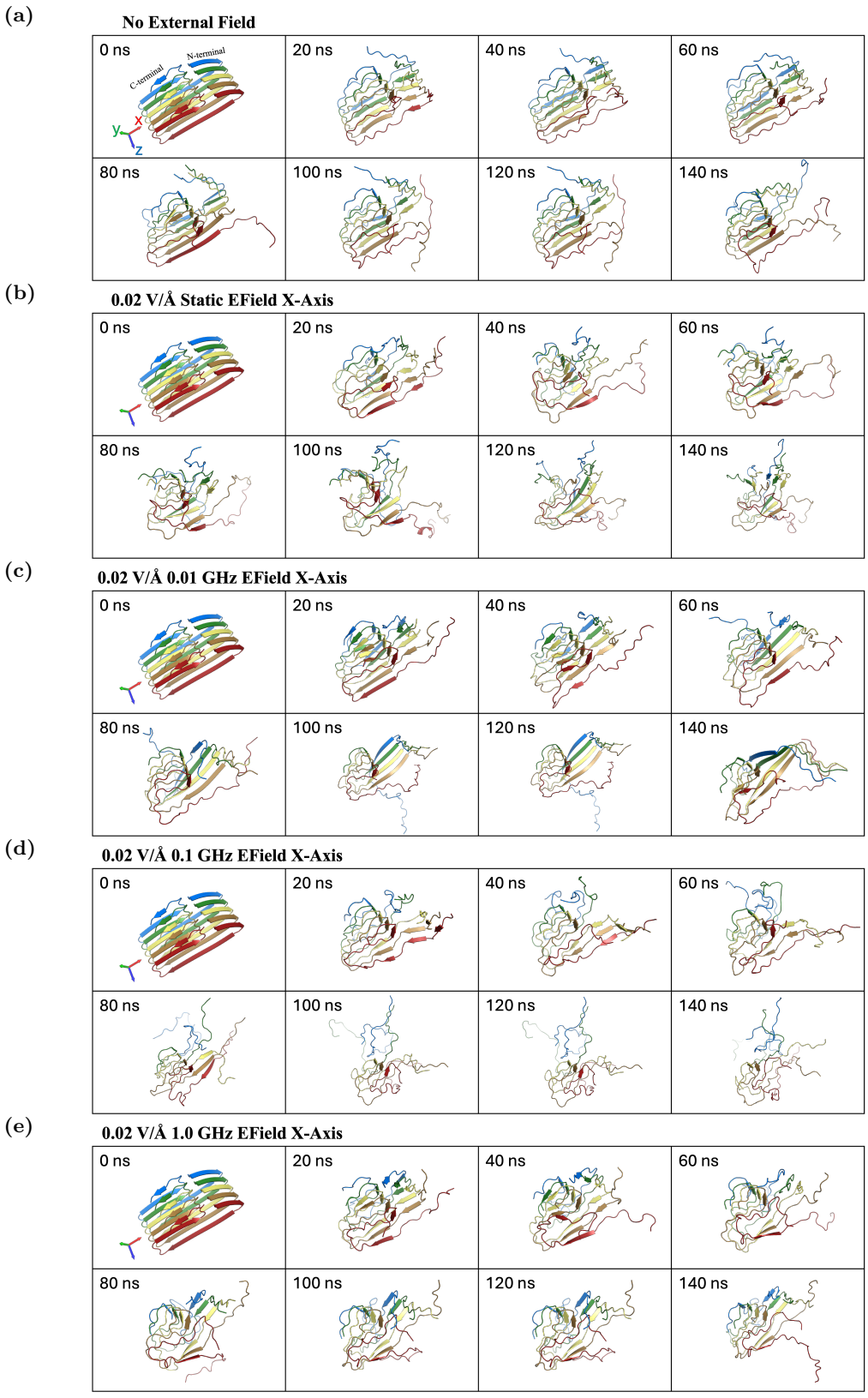

FIG. 3. Snapshots of amyloid beta 1–42 after 140 ns with external electric fields applied in the x direction. Panels show (a) no field, (b) a static field at 0.02 V/Å, and oscillating fields at 0.02 V/Å with frequencies (c) 0.01 GHz, (d) 0.1 GHz, and (e) 1 GHz.

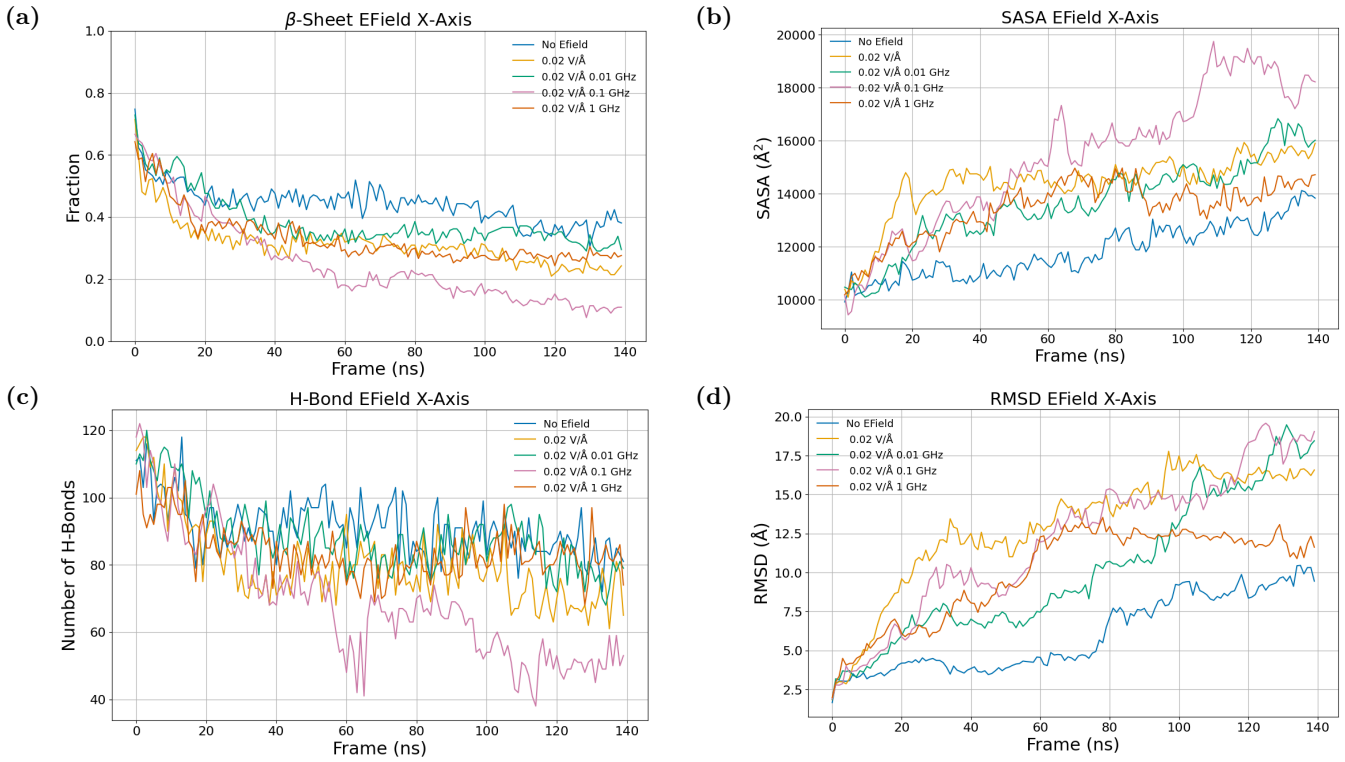

FIG. 4. Trajectory analysis of amyloid beta 1–42 under external electric fields applied along the x direction. Panels show the time evolution of structural metrics over the 140 ns simulations: (a) beta sheet fraction, (b) solvent-accessible surface area (Å^2), (c) number of hydrogen bonds, and (d) root mean square deviation (Å) from the initial structure. Each curve corresponds to simulations with no field, a static 0.02 V/Å field, or oscillating 0.02 V/Å fields at 0.01, 0.1, and 1 GHz.

CONCLUSION

In this work, we implemented the static and oscillating external electric fields for the polarizable force fields AMOEBA[12], AMOEBA+[13], and HIPPO[14] within the Tinker-CPU[15] and Tinker-GPU[16] packages. Because the molecular response depends on both electrostatics and polarization, polarizable force fields provide a physically consistent framework for external field simulations. We demonstrated two applications of external field simulations.

First, we computed the dielectric spectra of water and aqueous glucose using both fluctuation dissipation and direct field methods. The spectra captured features also seen in the experimental spectrum, including a decrease in magnitude and in frequency of the Debye peak of water as well as the presence of a low-frequency feature. Second, we observed a field-dependent structural disorder of the amyloid beta protein. The simulations reproduced the previously reported frequency dependent denaturation[17], with intermediate frequencies producing the greatest disorder.

Overall, these developments extend the Tinker platform to support external field simulations with advanced polarizable force fields and provide tools for analyzing molecular responses. The implementation enables future studies of dielectric response, spectroscopic observables, and biomolecular structural changes under the influence of an external field.

SUPPLEMENTARY MATERIAL

The supplementary material contains tables reporting the temperatures of pure water and aqueous salt under various field strengths, frequencies, and thermostat settings. It also includes the amyloid beta protein structure and disorder metrics for fields applied along the y- and z-axes. The input files used for the simulations in this study are provided in the supplementary files.

ACKNOWLEDGEMENTS

M.K.J.C. gratefully acknowledges support of this work by The Molecular Sciences Software Institute, under the NSF grant CHE-2136142. J.W.P. gratefully acknowledges support of this work by NIH NIGMS award R01 GM106137 from the U.S. National Institutes of Health. This article was prepared in part by Theiss Research using Federal funds under award 70NANB23H207 from the National Institute of Standards and Technology, U.S., Department of Commerce. The statements, findings, conclusions, and recommendations are those of the au-

thors and do not necessarily reflect the views of the National Institute of Standards and Technology or the U.S. Department of Commerce.

AUTHOR DECLARATIONS

Conflict of Interest

J. W. Ponder is a co-founder of Qubit Pharmaceuticals.

Author Contributions

Moses K. J. Chung: Conceptualization (equal); Data curation (equal); Formal analysis (equal); Investigation (equal); Methodology (equal); Software (equal); Validation (equal); Writing – original draft (equal); Writing – review & editing (equal). **Rebecca A. Bone**: Conceptualization (equal); Data curation (equal); Formal analysis (equal); Investigation (equal); Methodology (equal); Software (equal); Validation (equal); Writing – original draft (equal); Writing – review & editing (equal). **Zhi Wang**: Conceptualization (equal); Investigation (equal); Methodology (equal); Software (lead); Writing – original draft (supporting); Writing – review & editing (supporting). **Kathleen Schwarz**: Conceptualization (equal); Data curation (equal); Formal analysis (equal); Funding acquisition (equal); Investigation (equal); Methodology (equal); Project administration (equal); Resources (equal); Software (equal); Supervision (equal); Validation (equal); Writing – original draft (equal); Writing – review & editing (equal). **Jay W. Ponder**: Conceptualization (equal); Data curation (equal); Formal analysis (equal); Funding acquisition (equal); Investigation (equal); Methodology (equal); Project administration (equal); Resources (equal); Software (equal); Supervision (equal); Validation (equal); Writing – original draft (equal); Writing – review & editing (equal).

DATA AVAILABILITY

Tinker-CPU and Tinker-GPU are publicly available on GitHub at https://github.com/TinkerTools. Data supporting the findings of this study are available from the corresponding authors upon reasonable request.

Note: Certain software are identified in this paper to foster understanding. Such identification does not imply recommendation or endorsement by the National Institute of Standards and Technology, nor does it imply that the software identified is necessarily the best available for the purpose. Certain commercial equipment, instruments, or materials are identified in this paper in order to specify the experimental procedure adequately. Such identification is not intended to imply recommendation or endorsement by the National Institute of Standards and Technology, nor is it intended to imply that the materials or equipment identified are necessarily the best available for the purpose.

[1] Niall J. English and J. M. D. MacElroy. Hydrogen bonding and molecular mobility in liquid water in external electromagnetic fields. *J. Chem. Phys.*, 119:11806–11813, 2003.

[2] M. W. Evans. The effect of orthogonal electric fields on the molecular dynamics of liquid water, principle three of group theoretical statistical mechanics. *J. Mol. Liq.*, 48:1–7, 1991.

[3] Niall J. English and Conor J. Waldron. Perspectives on external electric fields in molecular simulation: progress, prospects and challenges. *Phys. Chem. Chem. Phys.*, 17:12407–12440, 2015.

[4] Stephen D. Fried and Steven G. Boxer. Measuring electric fields and noncovalent interactions using the vibrational Stark effect. *Acc. Chem. Res.*, 48:998–1006, 2015.

[5] Stephen D. Fried and Steven G. Boxer. Electric fields and enzyme catalysis. *Annu. Rev. Biochem.*, 86:387–415, 2017.

[6] Valerie Vaissier Welborn, Luis Ruiz Pestana, and Teresa Head-Gordon. Computational optimization of electric fields for better catalysis design. *Nat. Catal.*, 1:649–655, 2018.

[7] Riccardo Reale, Niall J. English, José-Antonio Garate, Paolo Marracino, Micaela Liberti, and Francesca Apollonio. Human aquaporin 4 gating dynamics under and after nanosecond-scale static and alternating electric-field impulses: A molecular dynamics study of field effects and relaxation. *J. Chem. Phys.*, 139, 2013.

[8] Shawn M Kathmann. Electric fields and potentials in condensed phases. *Phys. Chem. Chem. Phys.*, 23:23836–23849, 2021.

[9] Michael Woodcox, Avik Mahata, Aaron Hagerstrom, Angela Stelson, Chris Muzny, Ravishankar Sundararaman, and Kathleen Schwarz. Simulating dielectric spectra: A demonstration of the direct electric field method and a new model for the nonlinear dielectric response. *J. Chem. Phys.*, 158:124122, 2023.

[10] Rebecca A. Bone, Moses K. J. Chung, Jay W. Ponder, and Kathleen Schwarz. Chain formation and addition drive the Debye relaxation of methanol. *J. Phys. Chem. B*, 129:8946–8951, 2025.

[11] Michael A. Sauer, Taylor Colburn, Sthitadhi Maiti, Matthias Heyden, and Dmitry V. Matyushov. Linear and nonlinear dielectric response of intrinsically disordered proteins. *J. Phys. Chem. Lett.*, 15:5420–5427, 2024.

[12] Pengyu Ren and Jay W. Ponder. Polarizable atomic multipole water model for molecular mechanics simulation. *J. Phys. Chem. B*, 107:5933–5947, 2003.

[13] Chengwen Liu, Jean-Philip Piquemal, and Pengyu Ren. AMOEBA+ classical potential for modeling molecular interactions. *J. Chem. Theory Comput.*, 15:4122–4139, 2019.

[14] Joshua A. Rackers, Roseane R. Silva, Zhi Wang, and Jay W. Ponder. Polarizable water potential derived from a model electron density. *J. Chem. Theory Comput.*, 17:7056–7084, 2021.

[15] Joshua A. Rackers, Zhi Wang, Chao Lu, Marie L. Laury, Louis Lagardere, Michael J. Schnieders, Jean-Philip Piquemal, Pengyu Ren, and Jay W. Ponder. Tinker 8: Software tools for molecular design. *J. Chem. Theory Comput.*, 14:5273–5289, 2018.

[16] Zhi Wang and Jay W. Ponder. Tinker-GPU: Next generation of Tinker with GPU support. Available from https://github.com/TinkerTools/tinker-gpu, 2022.

[17] Surajit Kalita, David Danovich, and Sason Shaik. Origins of the superiority of oscillating electric fields for disrupting senile plaques: Insights from the 7-residue fragment and the full-length Aβ-42 peptide. *J. Am. Chem. Soc*, 147:2626–2641, 2025.

[18] Moses K. J. Chung, Zhi Wang, Joshua A. Rackers, and Jay W. Ponder. Classical exchange polarization: An anisotropic variable polarizability model. *J. Phys. Chem. B*, 126:7579–7594, 2022.

[19] L. Martínez, R. Andrade, E. G. Birgin, and J. M. Martínez. Packmol: a package for building initial configurations for molecular dynamics simulations. *J. Comput. Chem.*, 30(13):2157–2164, 2009.

[20] Luke A. Newman, Mackenzie G. Patton, Breyanna A. Rodriguez, Ethan W. Sumner, and Valerie Vaissier Welborn. Polarizable

AMOEBA force field predicts thin and dense hydration layer around monosaccharides. *Chem. Commun.*, 97:14431–14434, 2024.

[21] Glenn J. Martyna, Mark E. Tuckerman, Douglas J. Tobias, and Michael L. Klein. Explicit reversible integrators for extended systems dynamics. *Mol. Phys.*, 87:1117–1157, 1996.

[22] Giovanni Bussi, Davide Donadio, and Michele Parrinello. Canonical sampling through velocity rescaling. *J. Chem. Phys.*, 126:014101, 2007.

[23] Rebecca A. Bone, Moses K. J. Chung, Jay W. Ponder, Demian Riccardi, Chris Muzny, Ravishankar Sundararaman, and Kathleen Schwarz. A new method to calculate broadband dielectric spectra of solvents from molecular dynamics simulations demonstrated with polarizable force fields. *J. Chem. Phys.*, 161:064306, 2024.

[24] Roland Faller and Juan J. de Pablo. Constant pressure hybrid molecular dynamics–monte carlo simulations. *J. Chem. Phys.*, 116:55–59, 2002.

[25] Rebecca A. Bone and Kathleen Schwarz. Computational dielectric spectroscopy shows that water/methanol mixtures form hybrid hydrogen bonding networks. *J. Chem. Phys.*, 164:094502, 2026.

[26] Lothar Gremer, Daniel Schölzel, Carla Schenk, Elke Reinartz, Jörg Labahn, Raimond B. G. Ravelli, Markus Tusche, Carmen Lopez-Iglesias, Wolfgang Hoyer, Henrike Heise, Dieter Willbold, and Gunnar F. Schröder. Fibril structure of amyloid-β(1–42) by cryo–electron microscopy. *Science*, 358:116–119, 2017.

[27] Yue Shi, Zhen Xia, Jiajing Zhang, Robert Best, Chuanjie Wu, Jay W. Ponder, and Pengyu Ren. Polarizable atomic multipole-based AMOEBA force field for proteins. *J. Chem. Theory Comput.*, 9:4046–4063, 2013.

[28] M. Tuckerman, B. J. Berne, and G. J. Martyna. Reversible multiple time scale molecular dynamics. *J. Chem. Phys.*, 97:1990–2001, 1992.

[29] Robert T. McGibbon, Kyle A. Beauchamp, Matthew P. Harrigan, Christoph Klein, Jason M. Swails, Carlos X. Hernandez, Christian R. Schwantes, Lee-Ping Wang, Thomas J. Lane, and Vijay S. Pande. MDTraj: A modern open library for the analysis of molecular dynamics trajectories. *Biophys. J.*, 109:1528–1532, 2015.

[30] LLC Schrödinger. The PyMOL Molecular Graphics System. Available from http://www.pymol.org.

[31] Vasileios Balos, Patrick Mueller, Gerhard Jakob, Mathias Klaeui, and Mohsen Sajadi. Imprinting the complex dielectric permittivity into the spintronic terahertz emission. *Appl. Phys. Lett.*, 119:091104, 2021.

[32] J. Barthel, K. Bachhuber, R. Buchner, H. Hetzenauer, and M. Kleebauer. A computer-controlled system of transmission lines for the determination of the complex permittivity of lossy liquids between 8.5 and 90 GHz. *Ber. Bunsenges. Phys. Chem.*, 95:853–859, 1991.

[33] Zbigniew Czumaj. Absorption coefficient and refractive index measurements of water in the millimetre spectral range. *Mol. Phys.*, 69:787–790, 1990.

[34] D. Downing, H. D.; Williams. Optical constants of water in the infrared. *J. Geophys. Res.*, 80:1656–1661, 1975.

[35] G. M. Hale and M. R. Querry. Optical constants of water in the 200-nm to 200-µm wavelength region. *Appl. Opt.*, 12:555–563, 1973.

[36] U. Kaatze. Complex permittivity of water as a function of frequency and temperature. *J. Chem. Eng. Data*, 34:371–374, 1989.

[37] Keiichirio Shiraga, Yuichi Ogawa, and Naoshi Kondo. Hydrogen bond network of water around protein investigated with terahertz and infrared spectroscopy. *Biophys. J.*, 111:2629–2641, 2016.

[38] H. P. Schwan, R. J. Sheppard, and E. H. Grant. Complex permittivity of water at 25°C. *J. Chem. Phys.*, 64:2257–2258, 1976.

[39] J. K. Vij, D. R. J. Simpson, and O. E. Panarina. Far infrared spectroscopy of water at different temperatures: GHz to THz dielectric spectroscopy of water. *J. Molec. Liq.*, 112:125–135, 2004.

[40] Hans R. Zelsmann. Temperature dependence of the optical constants for liquid H_2O and D_2O in the far IR region. *J. Molec. Struct.*, 350:95–114, 1995.

[41] Masahito Nakamura, Takura Tajima, and Michiko Seyama. Broadband dielectric spectroscopy for quantitative analysis of glucose and albumin in multicomponent aqueous solution. *IEEE J. Electromagn. RF Microw. Med. Biol.*, 6:86–93, 2021.

[42] Masahito Nakamura, Yujiro Tanaka, Takuro Tajima, and Michiko Seyama. Noninvasive glucose measurement using electromagnetic waves: Photoacoustic spectroscopy and dielectric spectroscopy. *NTT Tech. Rev.*, 17:40–45, 2019.

[43] Yuan Tao, Bowen Yan, Nana Zhang, Mingfu Wang, Jianxin Zhao, Hao Zhao, Wei Chen, and Daming Fang. Dielectric determination of glucose solutions under microwave fields via a novel molecular dynamics simulation approach. *J. Food Eng.*, 316:110844, 2022.

[44] K. Fuchs and U. Kaatze. Dielectric spectra of mono- and disaccharide aqueous solutions. *J. Chem. Phys.*, 116:7137–7144, 2002.

[45] Hermann Weingärtner, Andrea Knocks, Stefan Boresch, Peter Höchtl, and Othmar Steinhauser. Dielectric spectroscopy in aqueous solutions of oligosaccharides: Experiment meets simulation. *J. Chem. Phys.*, 115:1463–1472, 2001.

[46] A. Arbe, P. Malo de Molina, F. Alvarez, B. Frick, and J. Colmenero. Dielectric susceptibility in liquid water: Microscopic insights from coherent and incoherent neutron scattering. *Phys. Rev. Lett.*, 117:185501, 2016.

[47] Guillaume Stirnemann and Damien Laage. Direct evidence of angular jumps during water reorientation through two-dimensional infrared anisotropy. *J. Phys. Chem. Lett.*, 1(10):1511–1516, 2010.

[48] J.-H. Guo, Y. Luo, S. Kashtanov, J.-E. Rubensson, D. K. Shuh, H. Ågren, and J. Nordgren. Molecular structure of alcohol-water mixtures. *Phys. Rev. Lett.*, 91:157401, 2003.

[49] Eilon D. Kirson, Zoya Gurvich, Rosa Schneiderman, Erez Dekel, Aviran Itzhaki, Yoram Wasserman, Rachel Schatzberger, and Yoram Palti. Disruption of cancer cell replication by alternating electric fields. *Cancer Res.*, 64:3288–3295, 2004.

[50] Joachim K. Krauss, Nir Lipsman, Tipu Aziz, Alexandre Boutet, Peter Brown, Jin Woo Chang, Benjamin Davidson, Warren M. Grill, Marwan I. Hariz, Andreas Horn, Michael Schulder, Antonios Mammis, Peter A. Tass, Jens Volkmann, and Andres M. Lozano. Technology of deep brain stimulation: current status and future directions. *Nat. Rev. Neurol.*, 17:75–87, 2021.

[51] Felipe P. Perez, Bryan Maloney, Nipun Chopra, Jorge J. Morisaki, and Debomoy K. Lahiri. Repeated electromagnetic field stimulation lowers amyloid-β peptide levels in primary human mixed brain tissue cultures. *Sci. Rep.*, 11:621, 2021.